CrossMark

SPECIAL SECTION: ORIGINAL ARTICLE

"Hot Spots" in the Climate System: New Developments in the Extratropical Ocean-Atmosphere Interaction Research

Early summertime interannual variability in surface and subsurface temperature in the North Pacific

Shigeki Hosoda[1] · Masami Nonaka[2] · Yoshikazu Sasai[1] · Hideharu Sasaki[2]

Abstract Vertical structures of early summer ocean temperature variability on interannual and longer time scales in the North Pacific (NP) are investigated based on observational data obtained by the Argo. In the central and especially eastern NP regions, temperature variance is large but limited to the shallower layer. Given shallow mixed layer isolated by strong stratification from the subsurface layer due to strong short wave radiation in summer, the limitation to the shallower layer is expected. On the contrary, temperature variability in the western NP region frequently extends several hundred meters in depth. In the western NP, longer time scale variability of temperature is also apparent as temperature difference before and after 2008. Solutions of an eddy-resolving ocean general circulation model strongly suggest that the temperature variability is associated with changes in the oceanic frontal structures that extend to subsurface layer: enhancement of the northern branch of Kuroshio Extension and associated weakened meridional temperature gradients to the south and north of the current after 2008. The deep structure of temperature variability apparently indicates that it is caused not by atmospheric thermal forcing, but by oceanic structure changes, and it is corroborated by the similar variability in the subsurface salinity field. Also, it is shown that atmospheric thermal forcing strongly affects early summer sea surface temperature variability in the eastern NP, but not in the western NP.

1 Introduction

While it had been considered that midlatitude oceans are just passively influenced by the atmospheric variability, their active roles in the climate system have been revealed in the last decade with improvement of high-resolution satellite observations and ocean and atmospheric model simulations (e.g., Kwon et al. 2010). Those studies have shown that oceanic frontal zones mainly associated with western boundary currents are key regions for oceanic roles for formation of long-term mean atmospheric storm tracks and then large-scale circulation (e.g., Nakamura et al. 2004, 2008; Minobe et al. 2008; Nonaka et al. 2009; Taguchi et al. 2009; Sampe et al. 2010; Ogawa et al. 2012, among others).

For the oceanic active roles in interannual to decadal variability of ocean and atmosphere, especially for the roles of ocean dynamics, it is crucial that subsurface oceanic variability can induce sea surface temperature (SST) anomalies, as in the El Niño/Southern Oscillation phenomena in the equatorial Pacific region. Such ocean-induced SST anomalies are also found in the oceanic frontal zones (Nonaka et al. 2006, 2008, among others), and can affect planetary boundary layer and modify surface winds (Nonaka and Xie 2003; O'Neill et al. 2003; Chelton et al. 2004; Xie 2004; Small et al. 2008, among others). Further, recent studies have shown that impacts of the oceanic

✉ Shigeki Hosoda
hosodas@jamstec.go.jp

[1] Research and Develop Center for Global Change, Japan Agency for Marine-Earth Science and Technology, 2-15 Natsushima-cho, Yokosuka, Kanagawa 237-0061, Japan

[2] Application Laboratory, Japan Agency for Marine-Earth Science and Technology, Yokohama, Kanagawa, Japan

🖄 Springer

variability are not limited to the boundary layer, but extend to the upper troposphere (Frankignoul et al. 2011; Taguchi et al. 2012; O'Reilly and Czaja 2014).

Because of the importance of the ocean-induced SST anomalies, large parts of these studies on midlatitude air–sea interactions focus on winter, when the surface mixed layer (ML) deepens and subsurface oceanic structures and their variability can affect the surface layer. For example, signal of temperature variations formed in the deep winter ML can be kept in the subsurface layer below the seasonal thermocline and re-emerge next winter (e.g., Namias and Born 1970; Alexander and Deser 1995, among others). For summer and autumn seasons, several studies have found atmospheric responses to oceanic structure (Tanimoto et al. 2009; Sasaki et al. 2012; Miyama et al. 2012) and its variability (Norris 2000; Tomita et al. 2007; Nakamura and Miyama 2014; Okajima et al. 2014).

It is well known that strong short wave radiation warms the surface layer in summer and makes shallow surface ML and strong stratification below it. Due to the strong stratification, it has been considered that subsurface layer is free from the surface thermal forcing (e.g., Namias and Born 1970; Alexander and Deser 1995). One may then consider that temperature anomalies found in the surface layer are limited to that layer, but vertical structures of temperature anomalies in summer have not been well investigated due to limited in situ observations, although the importance of mesoscale eddy activity (Sugimoto and Hanawa 2011) and Kuroshio Extension (KE) bifurcation (Sugimoto 2014) for temperature variability has been suggested for the upstream KE region. The Argo observation system (Argo Science Team 2001) developed in the last decade, however, has made it possible to investigate interannual variability in surface and subsurface temperature on the basin scale. Further, a recent, well-quality controlled data set of heat flux at the sea surface makes it possible for us to clarify the relationship between changes in subsurface temperature and atmospheric condition.

The purpose of the present study is then to investigate vertical structures of temperature anomalies in early summer and their possible mechanisms. We analyze mainly in situ observational data and also use ocean general circulation model (OGCM) results for investigation of possible mechanisms for the temperature anomalies, as spatial resolution of the observational data is still limited for such purpose. Variability in salinity is also examined in the present study, as this additional parameter is useful for interpretation of the results of the analyses. The question we investigate in this present study is rather simple, but may be important for considering possibilities of air–sea interaction in the mid-latitude North Pacific (NP) in early summer.

We describe the analyzed observational data and OGCM in Sect. 2. In Sect. 3, observed temperature variability are shown and its possible mechanisms are investigated; these are further discussed in Sect. 4. The results are summarized in Sect. 5.

2 Observational data and model

2.1 MOAA-GPV

We use monthly temperature and salinity objective analysis data, which fully cover the global ice-free ocean from 70°N to 70°S (grid point value of monthly objective analysis of Argo: MOAA GPV; Hosoda et al. 2008). The temperature and salinity data used for the MOAA GPV are mainly lots of profiling float data of the Argo obtained from the Argo Global Data Assembly Center, being conducted with real-time and delayed-mode quality controls on each profile and with achieved accuracies of ±2.5 dbar for pressure, ±0.005 °C for temperature, and ±0.01 psu for salinity (Argo Data Management Team 2002). The horizontal grid size of MOAA GPV is 1° × 1° with 25 vertical standard levels from surface to 2000 dbar, analyzed by a two-dimensional optimal interpolation method on pressure surfaces for temperature and salinity. The horizontal decorrelation radii of the optimal interpolation are set to capture long-term and basin scale variations occurring with latitude and depth.

In addition, we use global, gridded, delayed-time, merged (Ducet et al. 2000) sea surface height (SSH) anomaly field reference products (SSALTO/DUACS User Handbook 2011) distributed by Archiving, Validation and Interpretation of Satellite Oceanographic data (AVISO). The SSH data products are available on a regular 0.25° grid, and their monthly mean values are used in this study. Also, for sensible and latent heat fluxes, we use the products of objectively analyzed air–sea fluxes (OAFlux; Yu et al. 2008).

2.2 North Pacific OFES

In addition to the observed data, we also use an eddy-resolving OGCM to investigate detailed variability in oceanic frontal structures. We use the Modular Ocean Model 3 OGCM (Pacanowski and Griffies 2000) with substantial modifications added for optimal performance on the vector-parallel hardware system of Japan's Earth Simulator. This NP Ocean Model for the Earth Simulator (OFES) (Sasaki and Klein 2012) with sea ice (Komori et al. 2005) covers nearly the whole NP domain (20°S–66°N, 100°E–70°W) with a horizontal resolution of 0.1°. The model has 54 vertical levels with 5-m resolution just below the surface, and the maximum depth is 6065 m. First, we conducted a 30-year integration with long-term (1979–2004) mean six hourly forcing

(climatological integration), and then from its 16th year, a hindcast integration with six hourly atmospheric fields taken from the Japanese 25-year reanalysis (Onogi et al. 2007) was conducted from 1979 to 2012. The NP OFES is based on the same numerical code as the widely used quasi-global OFES (Masumoto et al. 2004; Sasaki et al. 2008), but includes a sea ice model and is driven by different atmospheric field.

3 Results

3.1 Observed variability

At the beginning, we show interannual variability of early summertime oceanic structure obtained from observational data. Figure 1 displays SST (temperature at 10 dbar) standard deviation (SD) in each of May–July based on a monthly
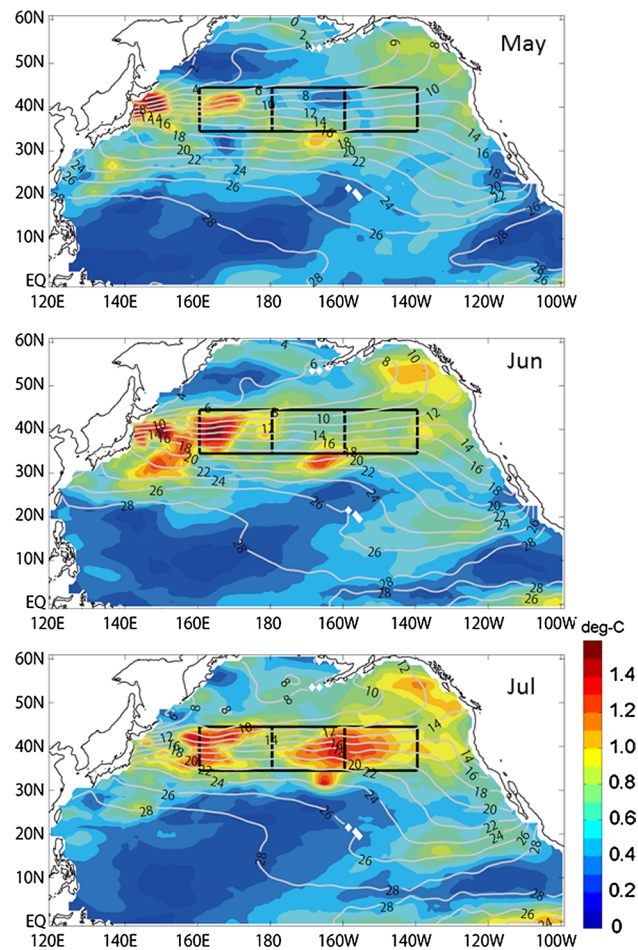
mean temperature field obtained from 2003 to 2012. Large SD areas widely and gradually spread from May to July around the 35°–45°N latitude band, where broad oceanic frontal zone with relatively higher meridional temperature gradient is formed between the subtropical and subpolar gyres. The SD larger than 1 °C continues during the early summer season, especially in the western region of the latitude band, while in the eastern region, the signal becomes large after July. In contrast, SDs in the western and central regions of subtropical and subpolar gyres are relatively small, <0.6 °C, emphasizing high interannual variability in SST in the latitude band of 35°–45°N. Note that in this study, we focus on the region to the east of 160°E, because in the upstream region of the KE, the importance of eddy activity west of 155°E (Sugimoto and Hanawa 2011), and of KE bifurcation in 155°–160°E (Sugimoto 2014) for temperature variability have been suggested.

In Fig. 2, we indicate subsurface temperature SD at 200 dbar from May to July during 2003–2012. Note that the level is generally positioned below the shallow seasonal
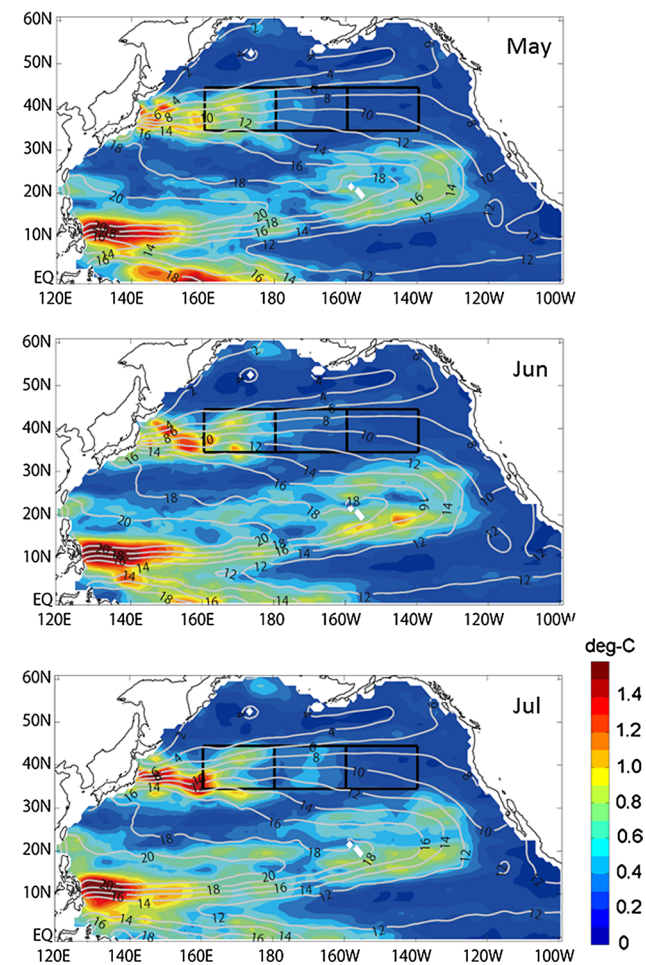

Fig. 1 Standard deviation (SD) of interannual SST variation in **a** May, **b** June and **c** July for 2003–2012 in NP obtained from MOAA GPV. *Gray contour* shows average temperature distribution for 2003–2012. *Rectangles* denote western (160°E–180°), central (180°–160°W) and eastern (160°–140°W) regions of the analyses area along 35°–45°N latitude band

Fig. 2 As in Fig. 1, except for subsurface temperature and its SD at 200 dbar

thermocline in the mid and high latitude of the NP. The larger SD in the subsurface layer appears around KE, below the western part of the high SST SD region (Fig. 1), and also in the western and central tropical region where impact of warm water pool migration associated with ENSO is dominant (Picault et al. 1996). On the contrary, the SD in the central and eastern regions of the 35°–45°N latitude band is rather small and is <0.5 °C during early summertime. This suggests that temperature anomalies in the eastern region (and somewhat also in the central region) are confined above the maximum winter ML depth, which is defined as a depth at which the σ_θ difference from it at 10 dbar is equal to 0.125 kg m^{-3} (MLD; shown below in Fig. 4), while temperature variability in the western region extends to the subsurface layer, indicating that the temperature variation mechanism in the western region could be different from that in the central and eastern regions.

To confirm the difference of the vertical distribution of temperature variability, we plot zonal sections of surface and subsurface temperature SD in May–July along the latitude band (35°–45°N) in Fig. 3. As found above, the vertical structure of temperature variability has clear zonal contrast; that is, deep coherent structure extending over 500 dbar far below MLD in the western region and very shallow high SD limited to upper 100 dbar in the eastern region. In the central region, the vertical structure is shallow, which is similar to the eastern region; however, some higher SDs can be seen to extend at least to a depth of 400 dbar.

For further clarification of interannual temperature variability in the surface and subsurface layer, time series of temperature anomalies are shown in Fig. 4, in each of the western, central and eastern regions of the latitude band. The deeper structures below the MLD are clearly found more in the western region (>500 dbar) than in the central (~400 dbar) and eastern regions (~200 dbar). While substantial interannual temperature variability appears in all regions, a clear shift from negative to positive anomalies can be found around 2008 in the western region, and it is also hinted in the central region. With regards to the seasonal evolution, subsurface anomaly formed by deep winter convection tends to be maintained during early summertime (especially May–July), not only in the subsurface, but also in the surface layer in the thin ML (e.g., 2007, 2009, and 2012). There are, however, years when early summer surface temperature has a sign opposite to that in the subsurface layer, showing that the connection between the subsurface and surface layers in summer is rather fragile compared to that in winter.

As discussed above, deep anomaly structure can be found and the sign of temperature anomaly clearly changed from negative to positive around 2008 in the western region. Here we investigate meridional structure of the
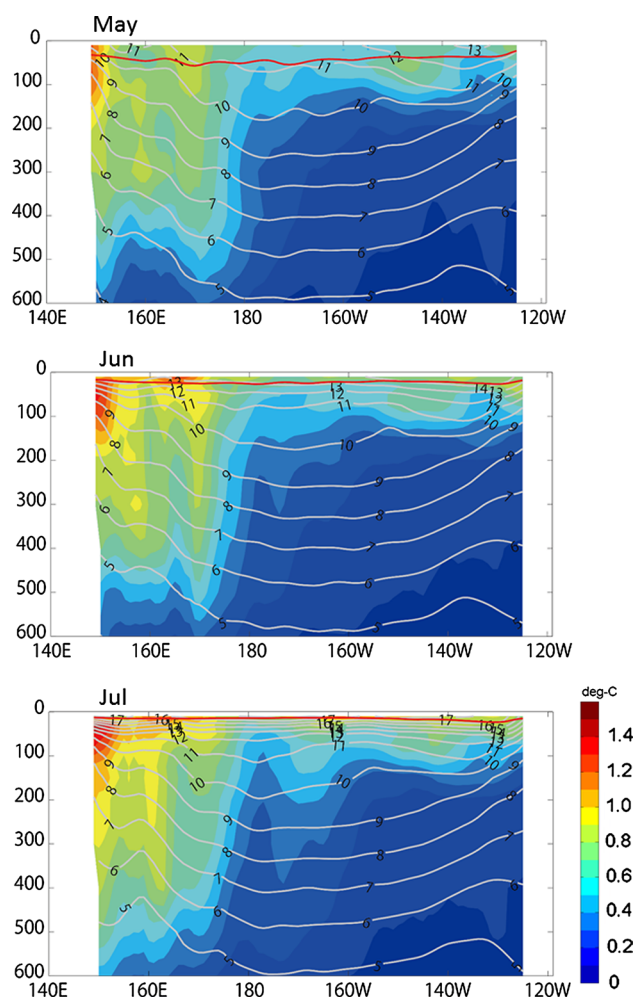

Fig. 3 As in Fig. 1, except for zonal sections of subsurface temperature and its SD along 35°–45°N latitudinal band. Monthly MLD is plotted as *red solid line*, which is defined as a depth at which σ_θ difference from σ_θ at 10 dbar equal to 0.125 kg m^{-3}

temperature difference between the two periods 2003–2007 and 2008–2012 in the western region (Fig. 5a). The most dominant positive temperature differences are found around 40°–45°N, and they extend several hundred meters in depth. Additionally, meridional local ridge of the difference is also found around 35°N around 300–400 dbar, although the difference in SST in this region is very limited. Further, it is hinted that the local trough of the difference is formed around 38°N at 300–400 dbar. While their distribution is rather diffusive, probably due to limited observation density even in the Argo era, Fig. 5a suggests that the dominant temperature differences exist around the subarctic and KE frontal zones.

To show the variability difference between surface and subsurface layers more clearly, we compare time series of surface and subsurface temperature in June (Fig. 6). In the surface layer (thick curves), high temperature values were

Fig. 4 Time–pressure plot of temperature anomaly (*color*) at 35°–45°N, **a** 160°–180°E, **b** 180°–160°W and **c** 160°–140°W. Anomaly is calculated based on monthly average temperature for 2003–2012. *Black contour* shows average temperature. MLD variation is plotted as *purple line*
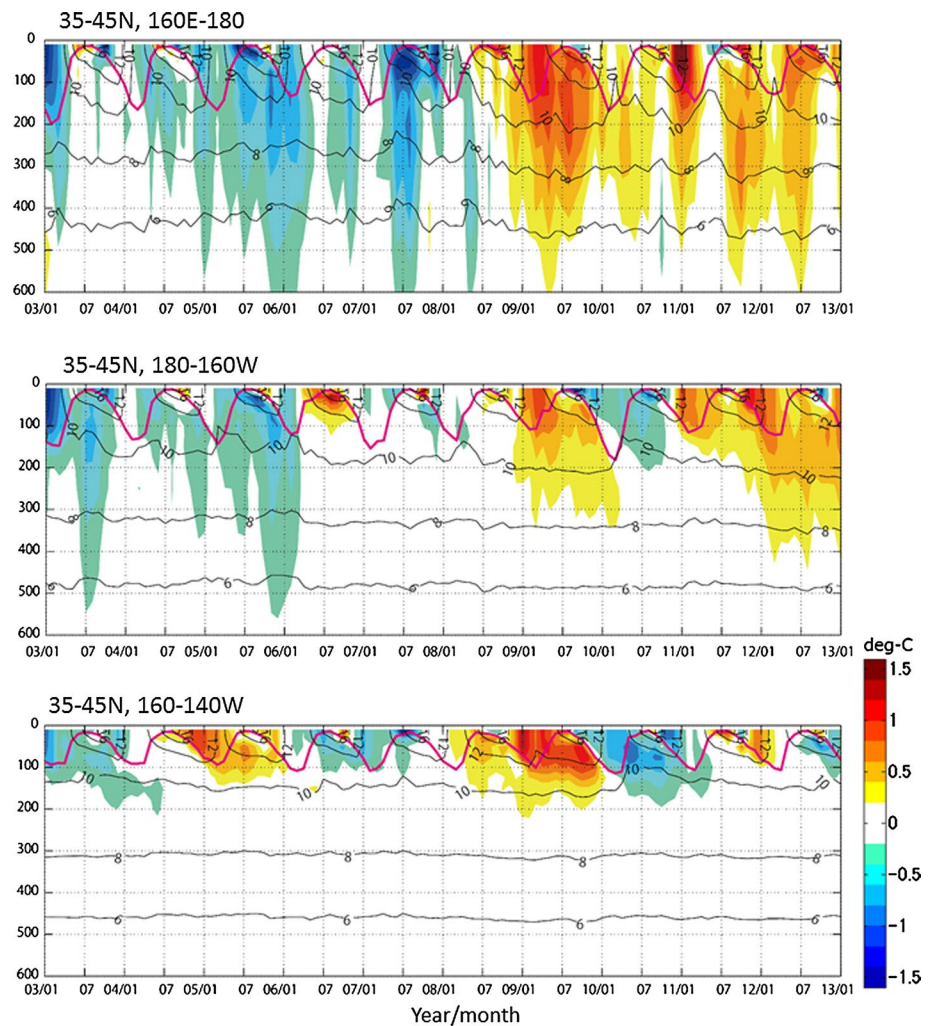
observed after 2008, except in 2011, as found in Fig. 4. This also corresponds with warm waters extending northward in the frontal zones after 2008 shown in Fig. 5a.

Then, we superimpose temperature anomaly in subsurface layer, at 200 (thin dotted curves) and 300 (thin dashed curves)-dbar depths as examples, to compare surface and subsurface variability. In the western NP region, subsurface temperature variability tends to have higher values after 2008 as in the surface layer. As the surface MLD is much shallower than 200 dbar in early summer in this region (see Fig. 3), thermal forcing at the sea surface cannot induce the subsurface temperature directly. Further, variability at 300-dbar depth, which is very similar to that at 200-dbar depth, confirms the subsurface temperature variability is not due to surface thermal forcing in winter, as 300 dbar is much deeper than the surface MLD in winter (Fig. 4, purple curves). Then, the rather similar variability in the surface and subsurface layer suggests that SST changes in this region can be induced by oceanic variability extending to the subsurface layer, although there are some exceptions

like 2011. In the central and eastern NP regions, in contrast, amplitudes of subsurface temperature variability are much smaller than the counterparts in the surface layer. This clearly shows that subsurface variability is not connected to the surface variability in these regions that are confined above maximum winter MLD (Fig. 4b, c).

3.2 Simulated variability

In the previous subsection, analyses of observed data suggest that high SST variability in the western region can be associated with subsurface oceanic structure changes. While it has been much improved thanks to Argo, resolution of observed data is still limited for examining changes in subsurface oceanic structure. In this subsection we examine it based on results of an eddy-resolving OGCM. First, we examine simulated temperature anomalies in the model. In Fig. 7, area-mean temperature anomalies in the western, central and eastern NP are shown to compare with the counterparts in the observed data (Fig. 4). With longer
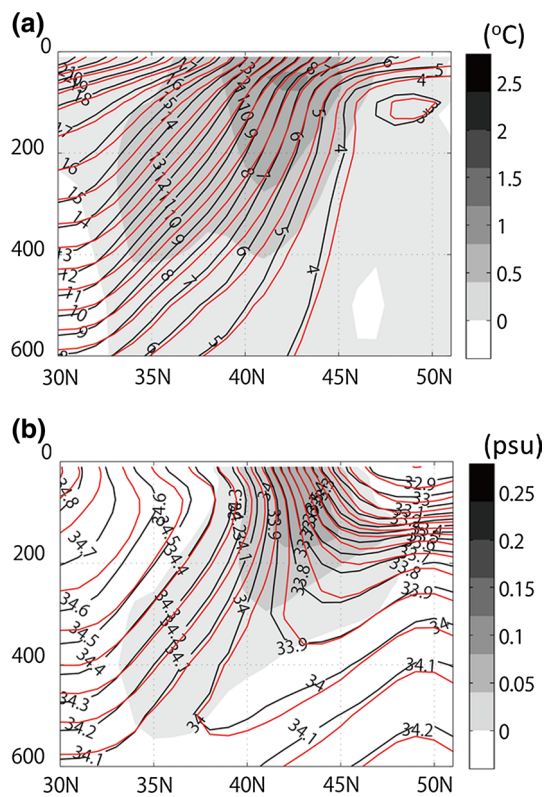
Fig. 5 a Zonal-mean annual-averaged meridional section of temperature in 160°–180°E in 2003–2007 (*black contours*) and 2008–2012 (*red contours*), and their difference (*shades* as indicated to the *right of the panel*) based on MOAA GPV. **b** Same as **a**, except for salinity field

Fig. 6 a Time series of area mean temperature (*black* in °C) anomalies at 10-dbar (*solid*), 200-dbar (*dotted*), and 300-dbar (*dashed*) depths in the western region (see Fig. 1; 35°–45°N, 160°E–180°) in June. **b** As in **a**, but for the central region (35°–45°N, 180°–160°W). **c** As in **a**, but for the eastern region (35°–45°N, 160°–140°W)

time series, the model depicts that the surface and subsurface temperature have interannual to decadal variability in the western and central NP, while the decadal one is obscure in the eastern NP. Also, consistent with the observations, there are deep temperature anomalies in the western NP, and surface and subsurface waters become warmer after 2008 compared to those in the period from 2003 to 2007, though simulated subsurface temperature variability tends to be larger than observed temperature in the central and eastern regions.

Then, as in the analysis for the observed data (Fig. 5), we examine difference fields between two 5-year periods after (2008–2012) and before (2003–2007) 2008, when the temperature change happened. Figure 8a indicates that warm temperature differences exist around 36°–38°N and 40°–44°N in the western NP, and extend to about 600 and 300 m depth, respectively, consistent with the deep structure of the temperature anomalies found in Fig. 7. Largely, these are consistent with the observed ones (Fig. 5), although the relative amplitude of temperature difference around 36°–38°N to that at 40°–44°N is higher compared to the observation. Also, in comparison with observational
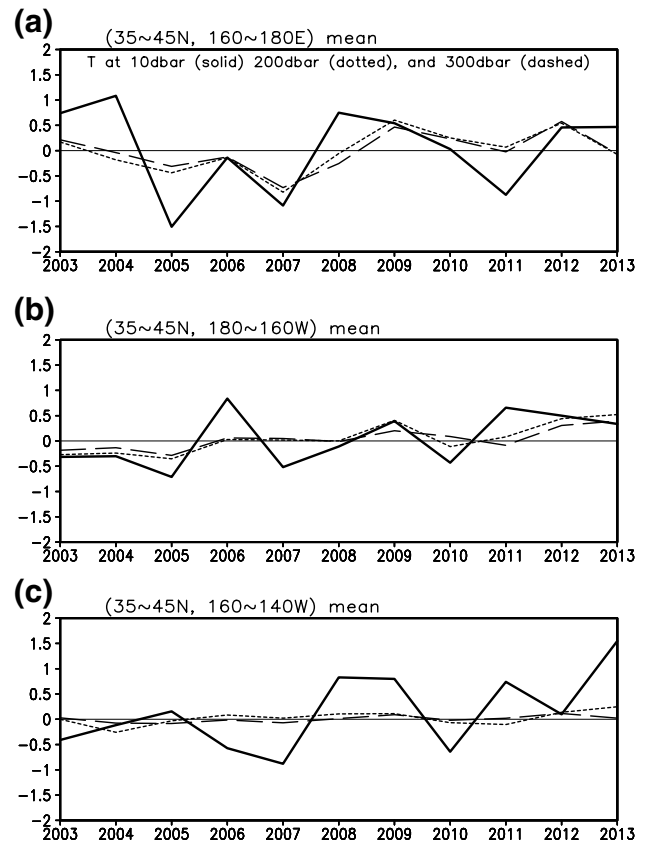
data, the model results depict sharper and clearer variability structure in the individual oceanic frontal zones. This is probably due to the rather diffusive oceanic structure found in the observed data with limited number of observations and wide spatial decorrelation radius, but at the same time, the simulated frontal structures may be exaggerated.

To consider reasons for the deep temperature anomalies found in the observation and model, we examine differences in meridional temperature gradient in the same region. In Fig. 8b and c, we plot the temperature gradient fields in the two periods before and after 2008, respectively. These plots indicate enhanced southward meridional temperature gradient around 38°N, and weakened ones around 36°N and 41°N after 2008. Also, almost no meridional shift is found in the subarctic frontal zone in the later 5-year period. Comparison of these changes in the temperature gradient with the temperature changes shows that the weakened temperature gradients around 36°N and 41°N are associated with northward extent of warmer subtropical water in the later period around 36°–38°N and 42°–44°N. Also, these warm anomalies are interrupted by

Fig. 7 (*Top panel*) Depth–time diagram of the area mean temperature in the western region (35°–45°N, 160°E–180°) based on the model solution. *Contours* (intervals are 2 °C) and *shades* (as indicated to the *right of the plot*) indicate temperature and temperature anomalies, respectively. The anomalies are departures from the mean from 1995 to 2012. (*Middle panel*) As in the top panel, except for the central region (35°–45°N, 180°–160°W). (*Bottom panel*) As in the top panel, except for the eastern region (35°–45°N, 160°–140°W)
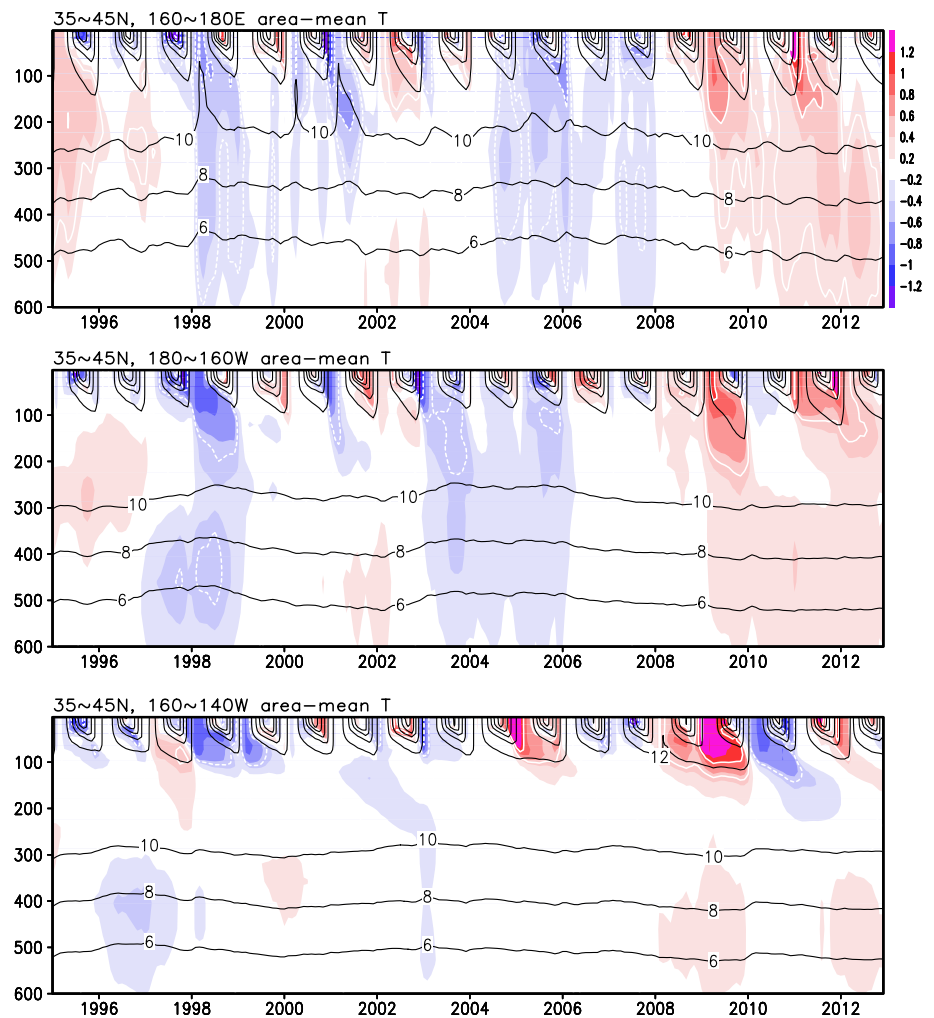

smaller temperature anomalies around 40°N to the north of the intensified gradient around 38°N. The strong temperature gradient around 38°N corresponds to the northern branch of KE (Mizuno and White 1983; Kida et al. 2015, for a recent review), and the branch is enhanced in the later period.

It should be noted that the warm temperature anomalies are not associated with northward migration of KE and subarctic frontal zones. This is different from what has been observed in this region in previous studies (Nonaka et al. 2006, 2008; Frankignoul et al. 2011; Taguchi et al. 2012), and rather consistent with what is found in the upstream KE (155°–160°E, Sugimoto 2014). Also, temperature difference in the KE front around 35°N is much weaker than that in the subarctic frontal zone. This finding is consistent with the lack of a coherent change between the KE front and subarctic front suggested by Nonaka et al. (2006) and Frankignoul et al. (2011). Further, it should be noted in the observation (Fig. 5), temperature difference in the subarctic frontal zone extends northward more than the simulated one (Fig. 8a).

In the central region, the frontal structure associated with temperature difference can be seen as in the western region, extending to a depth of 400 m (Fig. 9a). Although the structure of temperature difference is similar to the western region around 42°N, its meridional scale tends to be limited due to a narrower width of frontal zone. Around 34°–39°N, temperature difference appears at 300–600 m. Different from the western region, as meridional temperature gradient in this latitude band is not large in the central region (Fig. 9b, c), this temperature difference is probably not caused by change of frontal structure, and is rather associated with variation of thermocline depth. For the eastern part (Fig. 9d), we plot temperature difference between 2009 and 2010 because of the shorter time scale in the region (Figs. 4, 7c). The temperature difference is confined above 150 m, different from the western region. Also, the meridional temperature gradient is weak in the eastern region (Fig. 9b, c). In short, temperature variability in the eastern region is limited to the surface layer, and in the central region, the variability and also its mechanism are similar to those found in the western region only in the

Fig. 8 a Latitude–depth section of the simulated temperature fields (*contours*) and their difference (*shades*) zonally and annual averaged in the western region (160°–180°E). Contour intervals are 1 °C. **b, c** As in **a**, but for temperature fields (*contours*) and southward meridional temperature gradient (*shades* in K latitude^{-1} as indicated to the *right* of **c**) for **b** 2003–2007 mean and **c** 2008–2012 mean. **d–f** As in **a–c**, but for salinity field. Contour interval is 0.1 psu
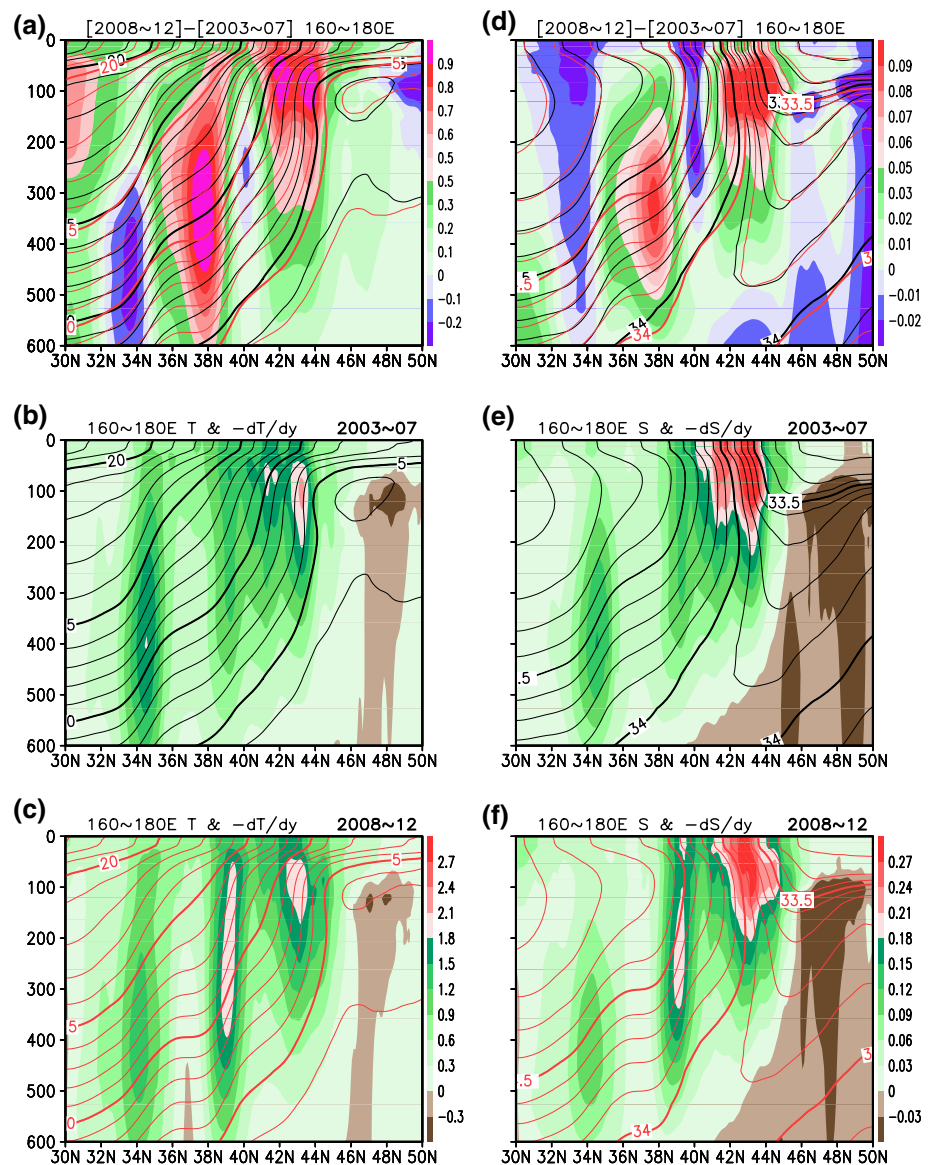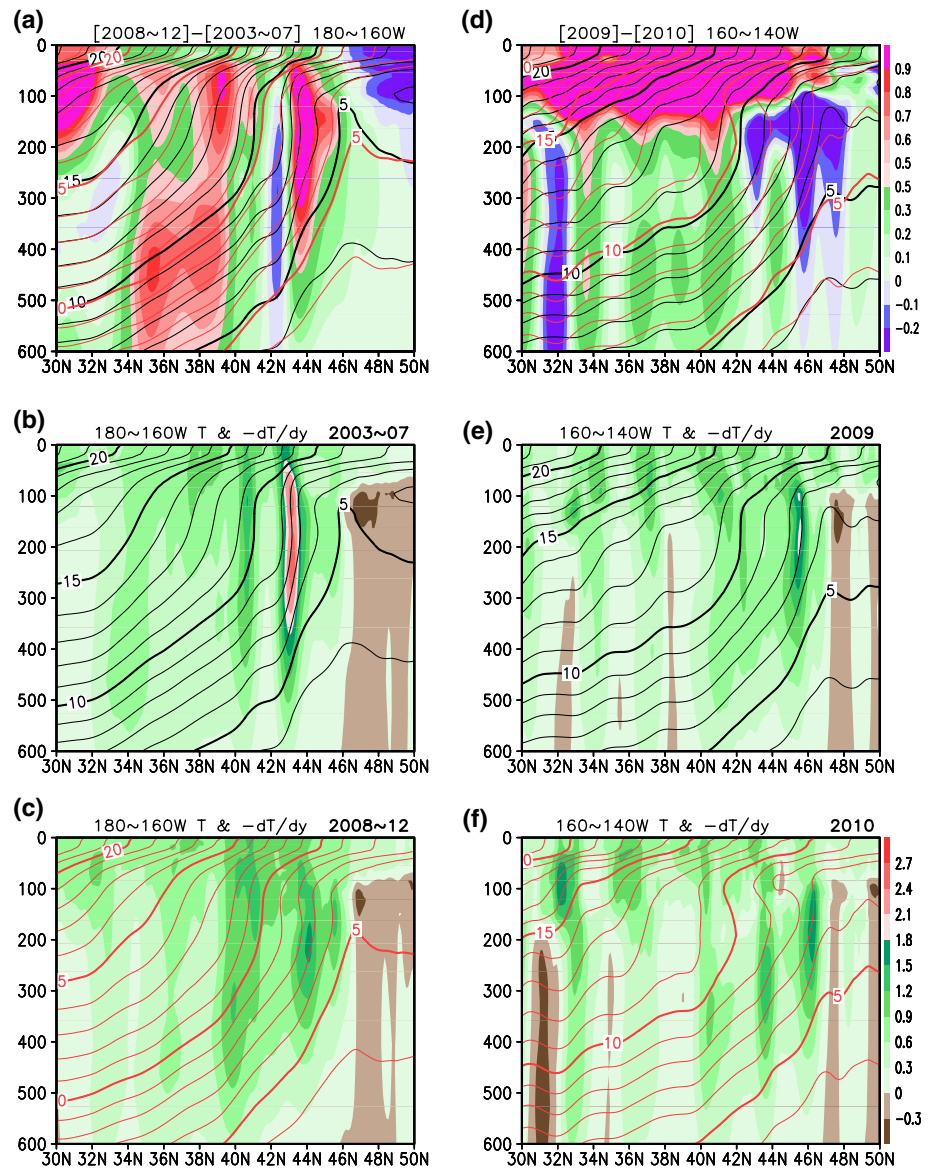

subarctic frontal zone, because of the meridional temperature structures.

The vertical extent to several hundred meters of the temperature variability found in the western region (and in the subarctic frontal zone in the central region) strongly suggests that it is not caused by direct influence of atmospheric thermal forcing at the sea surface. Supporting this, the corresponding plots for salinity field in the western region (Fig. 8d–f) show that the warm temperature anomalies are accompanied by higher salinity, and changes in the meridional salinity gradients are similar to those in the temperature field. These characteristics are consistent with those of observations, although a salinity difference at around 36°–38°N is stronger than in the observations (Fig. 5b). This clearly indicates that northward extension of warm and high salinity subtropical waters cause the warm temperature anomalies found in Fig. 8a.

The changes in temperature and salinity meridional gradients can be also found in the SSH field, as shown in Fig. 10. In the later period, intensified meridional SSH gradient corresponding to the northern branch of KE is clear around 38°N, and weakened SSH gradient is apparent to the south of it, whereas the northern weakened meridional SSH gradient is not clear in SSH (Fig. 10a, b). While it is less clear, the corresponding changes in SSH gradient were also hinted at in the satellite-observed SSH field (Fig. 10c, d). In the later period, meridional SSH gradient was intensified at around 37°N and weakened to the north and south of it. This implies that the observed temperature and salinity changes in Fig. 5 were induced by the changes in their frontal structure, as represented in the model. To confirm this, we plot latitude–time section of SSH meridional gradient for 20 years (Fig. 10e). Focusing on the period for a

Fig. 9 As in Fig. 8 **a–c**, except for the **a–c** central (180°–160°W), **d** temperature and the difference between 2010 and 2009, for **e** 2009 mean and **f** 2010 mean in the eastern (160°–140°W) regions


4 Discussion

4.1 Possible mechanism

To consider possible mechanisms for the changes in the frontal structures, we examined temporal development of SSH gradient field in the central to western NP based on the model solutions. While some possible relation with atmospheric circulation variability in winter is suggested, its meridional scale is much larger than that of the frontal structures and their change found in Fig. 8. Dynamical mechanisms for the frontal scale variability should be further investigated, and this is left for future studies.

As described in Sect. 3, the strong decadal-scale temperature change of the frontal zone in the western NP could be divided into two regions, the southern side around 36°–38°N and the northern side 40°–44°N extending to about 600 and 300 m, respectively (Figs. 5, 8). While the corresponding SSH difference is also hinted at by satellite in the southern side around 36°–38°N, the SSH difference in the northern side around 40°–44°N is rather obscure (see Fig. 10). This is because the northern side consists of stronger meridional temperature and salinity fronts than the southern one, and the temperature and salinity differences across the front tend to compensate each other their

decade from 2003 to 2012, meridional SSH gradient seems to be intensified around 32°N and 37°–38°N and to be weakened around 35°–36°N in the later 5 years, although there are meridional migrations in addition to the variability in the gradient.

Fig. 10 a Horizontal map for 2003–2007 mean SSH (contours with intervals of 10 cm) and its southward meridional gradient using OGCM (*shades* in cm latitude^{-1} as indicated at the *bottom* of **b**). **b** As in **a**, but for 2008–2012. **c** Meridional profiles for SSH meridional gradient zonally averaged in 160°–180°E for 2003–2007 mean (*black curve*) and 2008–2012 mean (*red curve*) using OGCM. **d** As in **c**, but for the satellite observed SSH. **e** Mean observed SSH (*contour*) and its meridional gradient (*shade* as indicated at the *bottom* of **b**) time series on 160°–180°E from 1993 to 2012. Contour interval is 10 cm
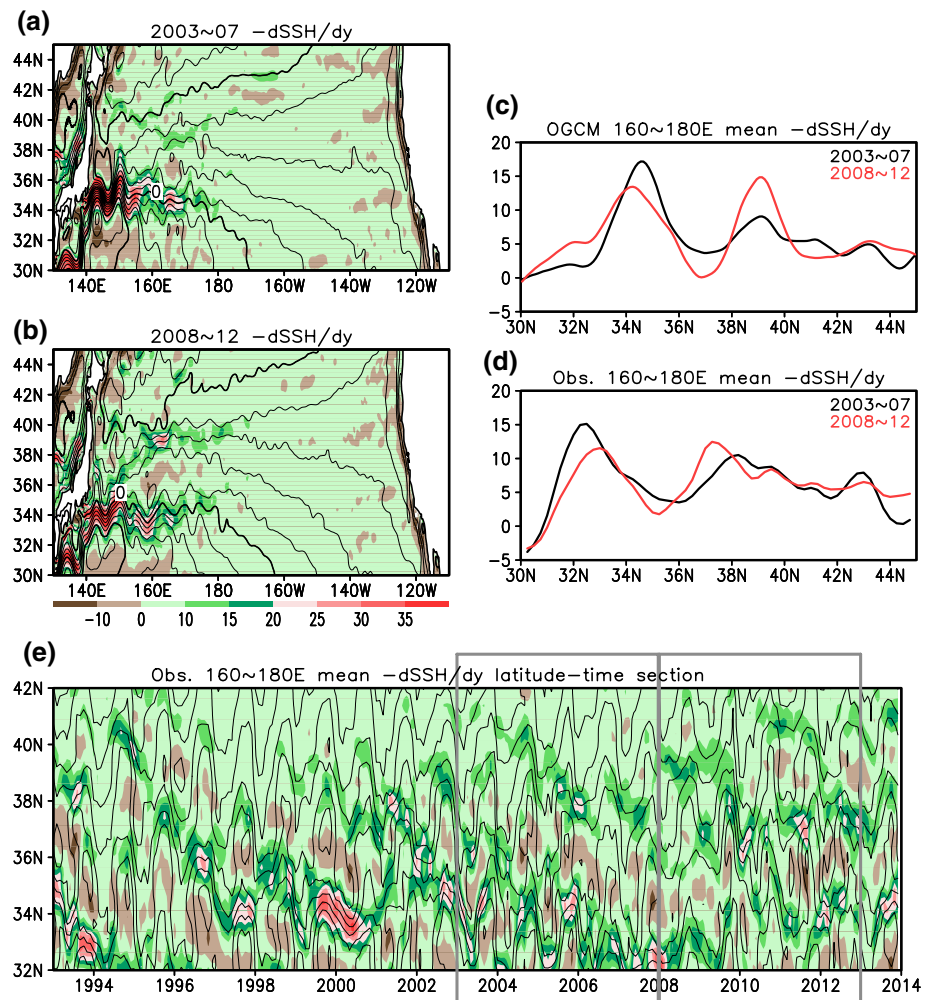

influence on density. The signal of SSH and its change in the northern part then become obscure.

The negative meridional SSH gradient (SSH increase northward) clearly found to the south of the northern branch of KE in the later period (Fig. 10b) indicates westward current and existence of recirculation to the south of the northern branch in the model. This implies that the weakened meridional temperature gradient around 36°N (Fig. 8c) and the resultant warmer temperature around 36°–38°N (Fig. 8a) are associated with the enhanced recirculation. Whether the strengthened northern branch can be associated with a recirculation gyre has not been studied yet; to our knowledge, it should be investigated in future to improve our understanding of variability in this region.

To quantitatively confirm the processes that induce the surface temperature variability found after 2008, we further investigate heat budget balance in the top 34 m in the three regions of NP. As the surface temperature anomalies developed at around 2006–2009 (Figs. 4, 7), we focus on this period, and to remove common seasonal variability, we examine the terms of heat budget relative

to the corresponding terms in 2006 (Fig. 11a–e, left panels). Also, as temperature anomalies are decided by temporal integration of temporal tendency, and temperature anomalies in early summer cannot be decided by the tendency in that season, in the following, we examine annual mean of each component of temperature tendency averaged in 2008 to investigate the warming from 2007 to early 2009. In the western region, temperature anomaly in the surface layer mainly develops in 2008 (average value relative to 2006 is 0.152×10^{-7} °C s^{-1}), and the advection and residual terms dominantly contribute to it (0.105 and 0.397×10^{-7} °C s^{-1}), while the surface heat flux is negative (-0.350×10^{-7} °C s^{-1}). As vertical mixing and diffusions cannot be estimated from output data files, the residual term includes horizontal and vertical diffusion, vertical mixing, and estimation errors. As surface temperature anomaly is smaller outside of the region (shown later in Fig. 14), horizontal diffusion affects to reduce the anomaly, and vertical diffusion and mixing would be dominant in the processes. Then, to interpret the residual term, we also examine heat budget balance for upper 68.2 m (Fig. 11f–j,

Fig. 11 a–e The heat budget term was averaged in the surface layer (0–34.3 m) in the western region (35°–45°N, 160°–180°E). Each term was calculated for 2007 (*red*), 2008 (*green*) and 2009 (*blue*) as the difference from the counterpart in 2006 based on the OFES monthly data. The panels consist of **a** sum of advection terms, **b** downward surface net heat flux, **c** residual term, **d** $\partial T/\partial t$ (*T* is temperature) and **e** temperature. The values written in the panels of **a**–**d** are annual mean for each year. Units are °C for temperature and 10^{-7} °C s^{-1} for others. **f–j** As in **a–e**, except for the near surface layer (0–68.2 m)
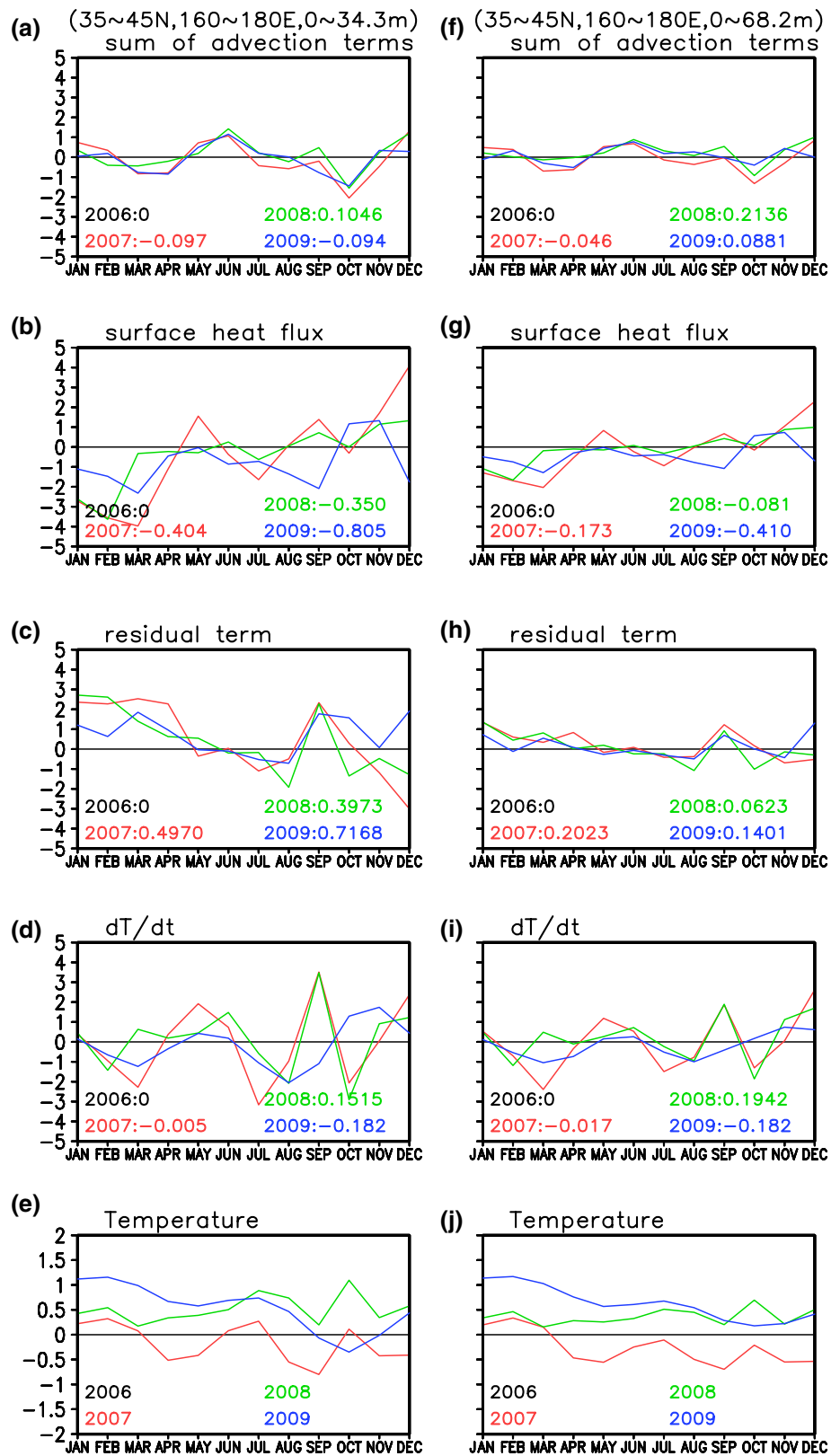
right panels). In this thicker layer, the advection terms are more dominant (0.214×10^{-7} °C s^{-1}; Fig. 11f) compared to that in the thin surface layer (0.105×10^{-7} °C s^{-1}; Fig. 11a) for the warming in 2008 (Fig. 11d, i), and the residual term is less dominant (0.062×10^{-7} °C s^{-1}; Fig. 11h). These results suggest that advection warms water

in the near surface layer, and vertical mixing and/or diffusion affects the warming in the surface layer, although the vertical mixing and diffusion cannot be estimated directly. Also, it is noteworthy that relative importance of each term for $\partial T/\partial t$ is different in each season. For the penetration of heat between subsurface and surface layers, the mechanism associated with submeso-scale activity may play a crucial role (e.g., Qiu et al. 2006).

Different from the western region, surface heat flux is dominant in the central region (Fig. 12a–e). Relative to 2006, temperature in the surface layer warms in 2007 and 2008 (0.127 and 0.106 × 10^{-7} °C s^{-1}) and advection (−0.421 and −0.294 × 10^{-7} °C s^{-1}) and residual (−0.323 and −0.159 × 10^{-7} °C s^{-1}) terms are negative, while surface heat flux are positive (0.872 and 0.561 × 10^{-7} °C s^{-1}), indicating that surface heat flux contributes to the temperature warming in the central part. Similar to the central part, surface heat flux is also dominant in the eastern region (Fig. 12f–j). Relative to 2006, surface layer temperature warms in 2007 and 2008 (0.512 and 0.639 × 10^{-7} °C s^{-1}) and advection term is slightly positive (0.093 and 0.025 × 10^{-7} °C s^{-1}), while residual term is negative (−0.486 and −0.555 × 10^{-7} °C s^{-1}). The surface heat flux is clearly positive in 2007 and 2008 (0.906 and 1.170 × 10^{-7} °C s^{-1}), indicating the dominant influence of surface heat flux in the eastern region. From these, the mechanism for increase of the surface layer temperature in the western region is apparently different from the central and eastern regions.

4.2 Possibility of air–sea interactions

If SST anomalies in the western region are induced by oceanic structure variability rather than atmospheric thermal forcing as indicated above, they may have some feedback to the atmosphere aloft as discussed in Sect. 1. To investigate this possibility, we examine interannual variability in SST and sensible and latent heat fluxes at the sea surface in June (Fig. 13). In the eastern region (Fig. 13c), interannual variability in SST (black curve) and surface heat flux anomalies (red and blue curves) tend to be out of phase. Also surface wind speed anomalies (orange curve) tend to be in (out) phase with surface heat flux (SST) anomalies, indicating that stronger winds induce higher sensible and latent heat fluxes and cool the ocean surface. In the central region (Fig. 13b), such relations are not clear, and so are in the western region (Fig. 13a), clearly different from those found in the eastern NP. Consistently, the heat fluxes do not have a clear relation with wind speed, again different from the relation found in the eastern region. Further, with detailed investigation of Fig. 13, we can find that SAT anomalies (green curve) tend to be smaller (larger) than SST anomalies in the western (eastern) region. While more

thorough investigations are necessary to clarify the reasons, these can happen if cool (warm) SAT is induced by cool (warm) SST in the western region and cool (warm) SST is induced by cool (warm) SAT in the eastern region. These relations, however, are not as clear in June as in other months. This suggests that some seasonality, for example, in the atmospheric circulation may be also important for ocean-to-atmospheric feedback in early summer in NP.

4.3 Horizontal distribution of SST and SSS difference

In Fig. 14, we examine horizontal distributions of changes in SST and SSS between the periods of 2008–2012 and 2003–2007. Over the central NP, there were warm anomalies after 2008, but cool anomalies were found along the eastern boundary region along North America and extended to the central to western part of the tropical Pacific, while there were substantial warm anomalies in the eastern equatorial Pacific. This SST anomaly pattern is similar to that corresponding to the negative phase of the El Niño Modoki (also called as the Central Pacific El Niño, the Warm Pool El Niño, etc.; Ashok and Yamagata 2009 and references therein). It is also noteworthy that cool SST anomalies were found in the western boundary region of NP.

Comparison with SSS anomalies shows that the synchronized changes in temperature and salinity found in the western NP region (Fig. 5) is not generally found. The SST and SSS difference after 2008 distribute in very different ways. The substantial SSS anomalies in the tropics correspond to those associated with the quasi-decadal variability discussed by Hasegawa et al. (2014).

5 Summary

Considering ocean to atmosphere feedback in midlatitude in summer, we examine vertical structure of temperature anomalies observed in NP in early summer based on in situ observational data and also an eddy-resolving OGCM. The observational data show apparent difference in the vertical structure of the temperature anomalies in the 2000s: they extend several hundred meters depth in the western region (35°–45°N, 160°–180°E), but are limited to the shallower layer in the central and eastern regions (35°–45°N, 180°–160°W, and 160°–140°W, respectively).

In summer, strong short wave radiation can warm the ocean from the surface and cause shallow ML and strong stratification at the bottom of it. Then, we can expect that the subsurface layer is insulated from the surface thermal forcing and that associated temperature anomalies are limited to the surface layer, and indeed, this is observed in the eastern region and somewhat in the central region. Although the analyses in the present study focus on interannual variability,

Fig. 12 **a–e** As in Fig. 11**a–e**, except for the central region (180°–160°W). **f–j** As in **a–e**, except for the eastern region (160°–140°W)
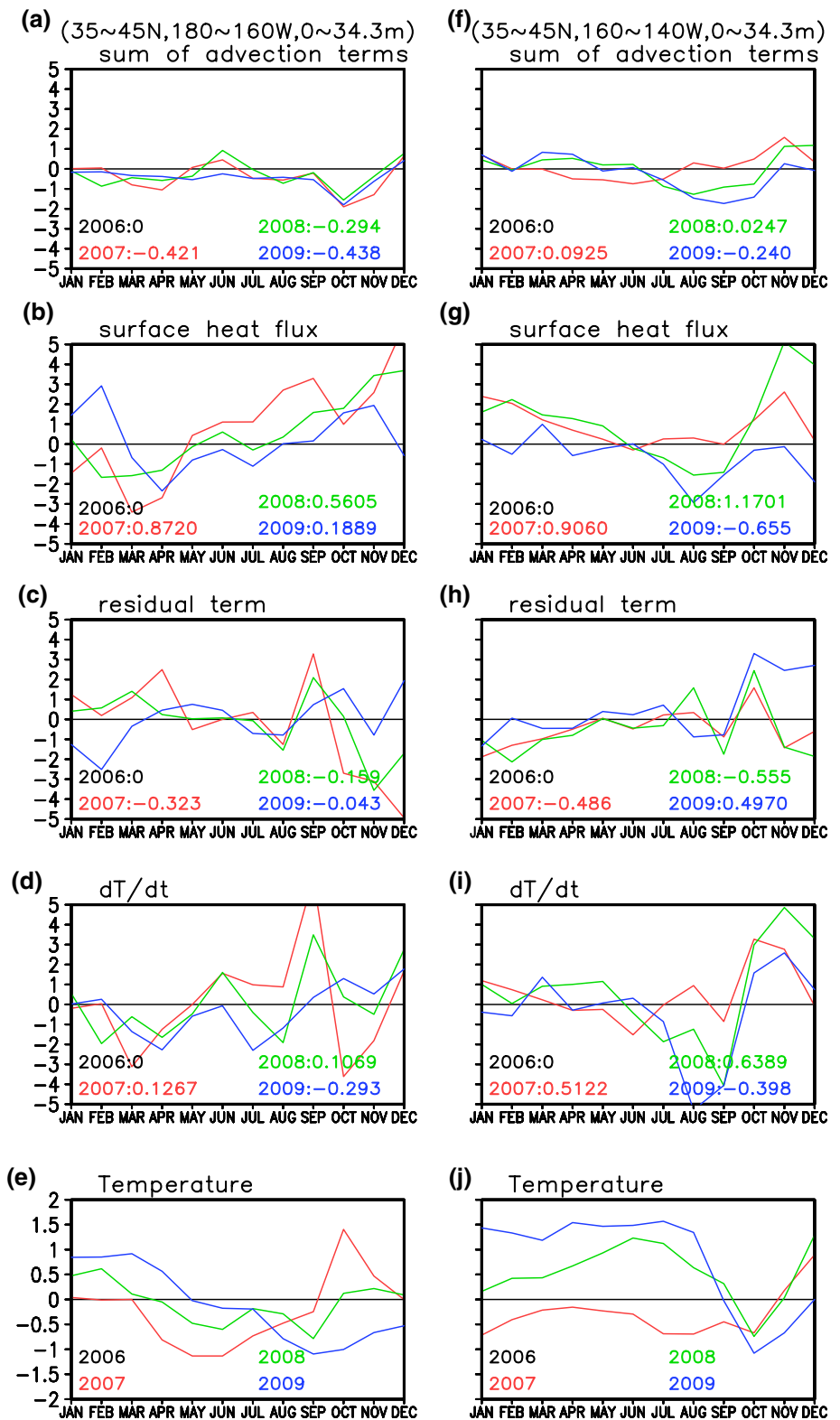
on a seasonal time scale, summer temperature variability induced by thermal forcing at the sea surface can penetrate downward below the strong seasonal thermocline even in the central and eastern parts of NP (Hosoda et al. 2015).

In the western region, in contrast, the surface and subsurface temperature variabilities cannot be separated even in early summer. The OGCM solution indicates that temperature anomalies in the western region are associated with

Fig. 13 **a** Time series of area annual-mean SST (*black* in °C with *left axis*), latent heat flux (*red* in W m^{-2} with *right red axis*), sensible heat flux (*blue* in W m^{-2} with *right red axis*), surface air temperature (*green* in °C with *left axis*), and surface wind speed (*orange* in m s^{-1} with *right orange axis*) anomalies in the western region (35°–45°N, 160°–180°E) in June. The upward heat fluxes are positive. **b** As in **a**, but for the central region (35°–45°N, 180°–160°W). **c** As in **a**, but for the eastern region (35°–45°N, 160°–140°W). SST is from MOAA GPV, other variables are from OAFlux
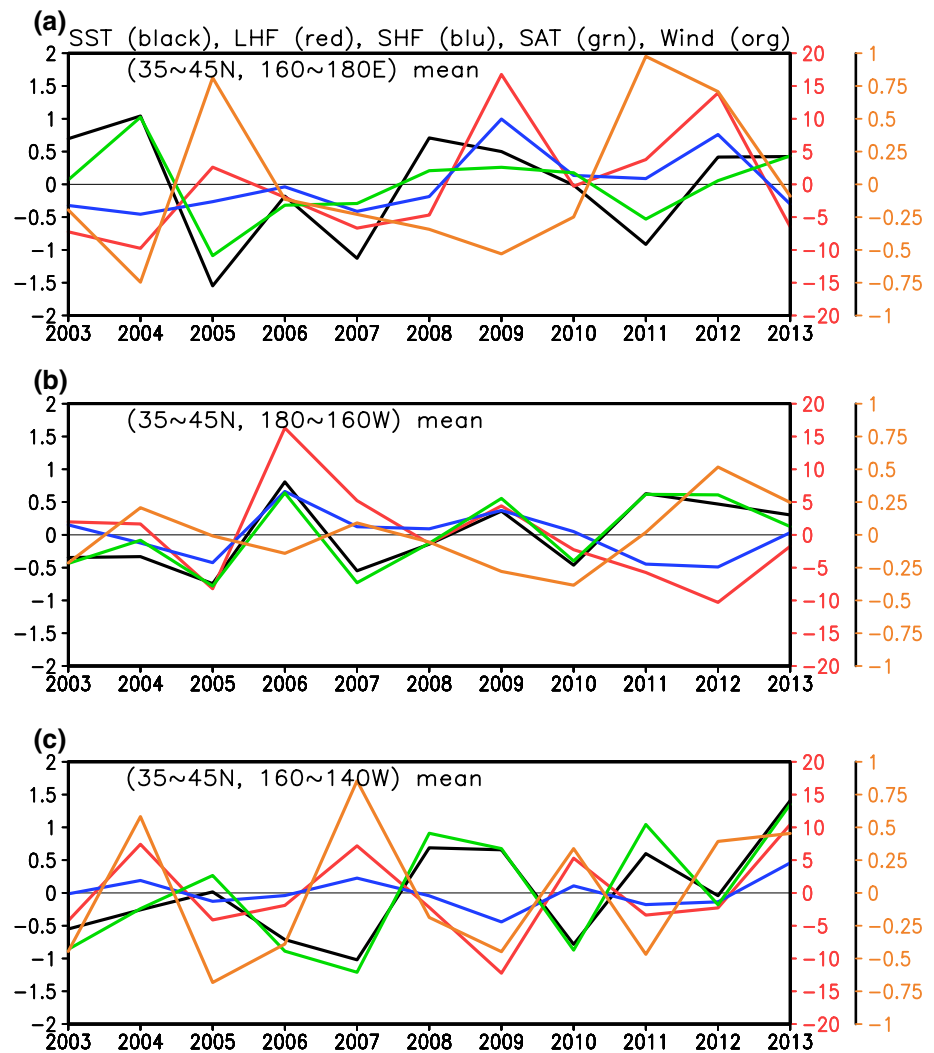
changes in the oceanic frontal structures that extend from the surface to the subsurface layer, and it is also supported by in situ observational data. Specifically, after 2008, the meridional temperature gradient is weakened (intensified) around 36°N and 41°N (38°N), and warmer waters extend northward, inducing the warm anomalies extending several hundred meters depth.

It is further confirmed that temperature tends to co-vary on interannual time scales in the surface and subsurface layers in the western region, but less in the central and eastern regions (Figs. 5, 6). As there are frontal structures not only in temperature but also in salinity in the western NP region, their co-variability (Fig. 5a, b) strongly suggests that the variability is caused by changes in the oceanic frontal structure as found in the OGCM solutions. In other words, these results strongly suggest that oceanic variability extending from the surface to the subsurface layer can induce SST variability even in early summer in the western region. Furthermore, comparison between SST anomalies and sea surface air temperature hints that the SST anomalies can modify

heat release from the ocean to the atmosphere, implying the possibility of ocean to atmosphere feedback even in warm seasons, consistent with a recent atmospheric model experiment (Okajima et al. 2014).

Although some possible linear relation between wind-stress curl variability and the northward extent of the sub-tropical warm water is suggested, its meridional scale is much larger than the oceanic frontal scale, and the mechanisms for the oceanic frontal structure changes are still not clear and further studies are necessary. Some nonlinear processes might operate as suggested for the KE jet in previous studies (Taguchi et al. 2005; Sasaki et al. 2013).

While it has been considered that midlatitude oceanic variability is passive to atmospheric variability especially in summer, the results in the present study indicate that at least in the western region of NP investigated here, the ocean can actively induce SST anomalies even in early summer. There may be such windows, through which the atmosphere can communicate with subsurface ocean variability (cf., Xie et al. 2000), in other regions. To deepen our

Fig. 14 **a** June SST difference between 2008–2012 mean and 2003–2007 mean (the former minus the latter; *shades* as indicated to the *right of the panel*) and 2008–2012 mean June SST (contours with intervals of 1 °C). **b** As in **a**, but for SSS (contour intervals are 0.1 psu). The *rectangles* indicate the western, central and eastern regions. Both SST and SSS are based on the MOAA GPV data
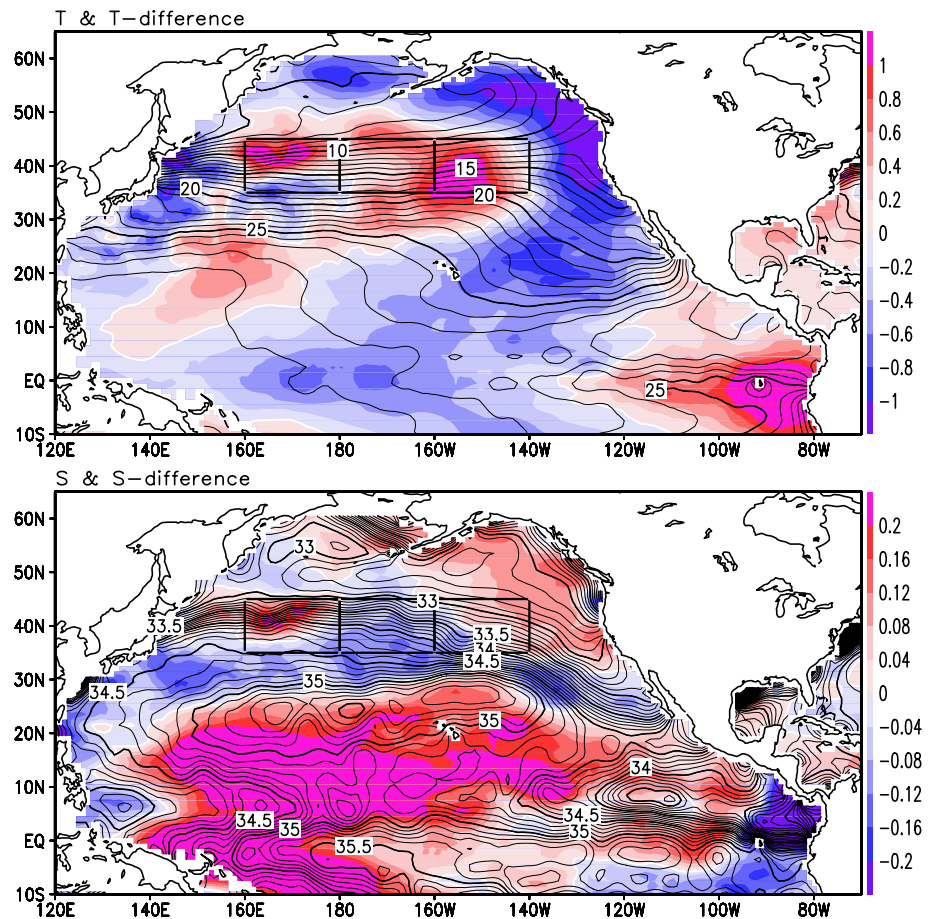
understanding of air–sea interactions in midlatitude, further investigations for such windows are necessary.

References

Alexander MA, Deser C (1995) A mechanism for the recurrence of wintertime midlatitude SST anomalies. J Phys Oceanogr 25:122–137

Argo Data Management Team (2002) Report of the Argo data management meeting. In: Proceedings of the Argo data management third meeting, marine environmental data, Ottawa, ON, Canada, p 42

Argo Science Team (2001) Argo: the global array of profiling floats. In: Koblinsky CJ, Smith NR (eds) Observing the oceans in the 21st century. GODAE Project Office, Bureau of Meteorology, Melbourne, pp 248–258

Ashok K, Yamagata T (2009) The El Nino with a difference. Nature 461:481–484

Chelton DB, Schlax MG, Freilich MH, Millif RF (2004) Satellite measurements reveal persistent small-scale features in ocean winds. Science 303:978–983

Ducet N, Le Traon P-Y, Reverdin G (2000) Global high resolution mapping of ocean circulation from TOPEX/Poseidon and ERS-1 and -2. J Geophys Res 105:19477–19498

Frankignoul C, Sennechael N, Kwon Y-O, Alexander MA (2011) Influence of the meridional shifts of the Kuroshio and the Oyashio Extensions on the atmospheric circulation. J Clim 24:762–777. doi:10.1175/2010JCLI3731.1

Hasegawa T, Ando K, Ueki I, Mizuno K, Hosoda S (2014) Upper-ocean salinity variability in the tropical pacific: case study for quasi-decadal shift during the 2000s using TRITON buoys and Argo floats. J Clim 26:8126–8138. doi:10.1175/JCLI-D-12-00187.1

Hosoda S, Ohira T, Nakamura T (2008) A monthly mean dataset of global oceanic temperature and salinity derived from Argo float observations. JAMSTEC Rep Res Dev 8:47–59

Hosoda S, Nonaka M, Tomita T, Taguchi B, Tomita H, Iwasaka N (2015) Impact of downward heat penetration below shallow seasonal thermocline on sea surface temperature. J Oceanogr. doi:10.1007/s10872-015-0275-7

Kida S et al (2015) Oceanic fronts and jets around Japan—a review. J Oceanogr. doi:10.1007/s10872-015-0283-7

Komori N, Takahashi K, Komine K, Motoi T, Zhang X, Sagawa G (2005) Description of sea-ice component of coupled ocean–sea-ice model for the Earth Simulator (OIFES). J Earth Simul 4:31–45

Kwon Y-O, Alexander MA, Bond NA, Frankignoul C, Nakamura H, Qiu B, Thompson L (2010) Role of the Gulf Stream and Kuroshio–Oyashio systems in large-scale atmosphere–ocean interaction: a review. J Clim 23:3249–3281. doi:10.1175/2010JCLI3343.1

Masumoto Y, Sasaki H, Kagimoto T, Komori N, Ishida A, Sasai Y, Miyama T, Motoi T, Mitsudera H, Takahashi K, Sakuma H, Yamagata T (2004) A fifty-year eddy-resolving simulation of the World Ocean: preliminary outcomes of OFES (OGCM for the Earth Simulator). J Earth Simul 1:35–56

Minobe S, Kuwano-Yoshida A, Komori N, Xie S-P, Small RJ (2008) Influence of the Gulf Stream on the troposphere. Nature 452:206–209. doi:10.1038/nature06690

Miyama T, Nonaka M, Nakamura H, Kuwano-Yoshida A (2012) A striking early-summer event of a convective rainband persistent along the warm Kuroshio in the East China Sea. Tellus A 64:1–9. doi:10.3402/tellusa.v64i0.18962

Mizuno K, White WB (1983) Annual and interannual variability in the Kuroshio Current system. J Phys Oceanogr 13:1847–1867

Nakamura M, Miyama T (2014) Impacts of the Oyashio temperature front on the regional climate. J Clim 27:7861–7873. doi:10.1175/JCLI-D-13-00609.1

Nakamura H, Sampe T, Tanimoto Y, Shimpo A (2004) Observed associations among storm track, jet streams and midlatitude oceanic fronts. In: Wang C, Xie S-P, Carton JA (eds) Earth's climate: the ocean–atmosphere interaction, geophysical monograph series, vol 147. AGU, Washington, D.C., pp 329–345

Nakamura H, Sampe T, Goto A, Ohfuchi W, Xie S-P (2008) On the importance of midlatitude oceanic frontal zones for the mean state and dominant variability in the tropospheric circulation. Geophys Res Lett 35(15):L15709. doi:10.1029/2008GL34010

Namias J, Born RM (1970) Temporal coherence in North Pacific sea-surface temperature patterns. J Geophys Res 75. doi:10.1029/JC075i030p05952

Nonaka M, Xie S-P (2003) Covariations of sea surface temperature and wind over the Kuroshio and its extension: evidence for ocean-to-atmosphere feedback. J Clim 16:1404–1413

Nonaka M, Nakamura H, Tanimoto Y, Kagkimoto T, Sasaki H (2006) Decadal variability in the Kuroshio–Oyashio Extension simulated in an eddy-resolving OGCM. J Clim 19:1970–1989

Nonaka M, Nakamura H, Tanimoto Y, Kagkimoto T, Sasaki H (2008) Interannual-to-decadal variability in the Oyashio and its influence on temperature in the subarctic frontal zone: an eddy-resolving OGCM simulation. J Clim 21:6283–6303

Nonaka M, Nakamura H, Taguchi B, Komori N, Kuwano-Yoshida A, Takaya K (2009) Air–sea heat exchanges characteristic of a prominent midlatitude oceanic front in the south Indian ocean as simulated in a high-resolution coupled GCM. J Clim 22:6515–6535

Norris JR (2000) Interannual and interdecadal variability in the storm track, cloudiness, and sea surface temperature over the summertime North Pacific. J Clim 13:422–430

O'Neill LW, Chelton DB, Esbensen SK (2003) Observations of SST-induced perturbations of the wind stress field over the Southern Ocean on seasonal time scales. J Clim 16:2340–2354

O'Reilly CH, Czaja A (2014) The response of the pacific storm track and atmospheric circulation to Kuroshio Extension variability. Q J R Meteorol Soc. doi:10.1002/qj.2334

Ogawa F, Nakamura H, Nishii K, Miyasaka T, Kuwano-Yoshida A (2012) Dependence of the climatological axial latitudes of the tropospheric westerlies and storm tracks on the latitude of an extratropical oceanic front. Geophys Res Lett 39:L05804. doi:10.1029/2011GL049922

Okajima S, Nakamura H, Nishii K, MiyasakaI T, Kuwano-Yoshida A (2014) Assessing the importance of prominent warm SST anomalies over the midlatitude North Pacific in forcing large-scale atmospheric anomalies during 2011 summer and autumn. J Clim 27:3889–3903

Onogi K et al (2007) The JRA-25 reanalysis. J Meteorol Soc Jpn 85:369–432

Pacanowski RC, Griffies SM (2000) MOM 3.0 manual. Geophysical Fluid Dynamics Laboratory/National Oceanic and Atmospheric Administration, p 680

Picault J, Ioualalen M, Menkes C, Delcroix T, McPhaden MJ (1996) Mechanism of the zonal displacements of the Pacific warm pool: implications for ENSO. Science 274:1486–1489

Qiu B, Hacker P, Chen S, Donohue KA, Watts DR (2006) Observations of the subtropical mode water evolution from the Kuroshio Extension system study. J Phys Oceanogr 36:457–472

Sampe T, Nakamura H, Goto A, Ohfuchi W (2010) Significance of a midlatitude oceanic frontal zone in the formation of a storm track and an eddy-driven westerly jet. J Clim 23:1793–1814

Sasaki H, Klein P (2012) SSH wavenumber spectra in the North Pacific from a high-resolution realistic simulation. J Phys Oceanogr 42:1233–1241. doi:10.1175/JPO-D-11-0180.1

Sasaki H, Nonaka M, Masumoto Y, Sasai Y, Uehara H, Sakuma H (2008) An eddy-resolving hindcast simulation of the quasi-global ocean from 1950 to 2003 on the Earth Simulator. In: Hamilton K, Ohfuchi W (eds) High resolution numerical modelling of the atmosphere and ocean. Springer, Berlin, pp 157–185

Sasaki YN, Minobe S, Asai T, Inatsu M (2012) Influence of the Kuroshio in the East China Sea on the early summer (Baiu) rain. J Clim 27:6627–6645

Sasaki YN, Minobe S, Schneider N (2013) Decadal response of the Kuroshio Extension jet to Rossby waves: observation and thin-jet theory. J Phys Oceanogr 43:442–456

Small RJ, de Szoeke SP, Xie S-P, O'Neill L, Seo H, Song Q, Cornillon P, Spall M, Minobe S (2008) Air–sea interaction over ocean fronts and eddies. Dyn Atmos Oceans 45:274–319

SSALTO/DUACS User Handbook (2011) (M)SLA and (M)ADT near-real time and delayed time products. CLS-DOS-NT-06-034, Issue 4.2

Sugimoto S (2014) Influence of SST anomalies on winter turbulent heat fluxes in the Eastern Kuroshio–Oyashio confluence region. J Clim 27:9349–9358. doi:10.1175/JCLI-D-14-00195.1

Sugimoto S, Hanawa K (2011) Roles of SST anomalies on the wintertime turbulent heat fluxes in the Kuroshio–Oyashio confluence region: influences of warm eddies detached from the Kuroshio Extension. J Clim 24:6551–6561

Taguchi B, Xie S-P, Mitsudera H, Kubokawa A (2005) Response of the Kuroshio Extension to Rossby waves associated with the 1970s climate regime shift in a high-resolution ocean model. J Clim 18(15):2979–2995

Taguchi B, Nakamura H, Nonaka M, Xie S-P (2009) Influences of the Kuroshio/Oyashio Extensions on air–sea heat exchanges and storm-track activity as revealed in regional atmospheric model simulations for the 2003/04 cold season. J Clim 22:6536–6560

Taguchi B, Nakamura H, Nonaka M, Komori N, Kuwano-Yoshida A, Takaya K, Goto A (2012) Seasonal evolutions of atmospheric response to decadal SST anomalies in the North Pacific subarctic frontal zone: observations and a coupled model simulation. J Clim 25:111–139

Tanimoto Y, Xie S-P, Kai K, Okajima H, Tokinaga H, Murayama T, Nonaka M, Nakamura H (2009) Observations of marine atmospheric boundary layer transitions across the summer Kuroshio Extension. J Clim 22:1360–1374

Tomita T, Sato H, Nonaka M, Hara M (2007) Interdecadal variability of the early summer surface heat flux in the Kuroshio region and its impact on the Baiu frontal activity. Geophys Res Lett 34, L10708. doi:10.1029/2007GL029676

Xie S-P (2004) Satellite observations of cool ocean–atmosphere interaction. Bull Am Meteorol Soc 85:195–208

Xie S-P, Kunitani T, Kubokawa A, Nonaka M, Hosoda S (2000) Inter-decadal thermocline variability in the North Pacific for 1958–97: a GCM simulation. J Phys Oceanogr 30:2798–2813

Yu L, Jin X, Weller RA (2008) Multidecade global flux datasets from the objectively analyzed air–sea fluxes (OAFlux) project: latent and sensible heat fluxes, ocean evaporation, and related surface meteorological variables. Woods Hole Oceanographic Institution, OAFlux Project Technical Report. OA-2008-01, Woods Hole, MA, p 64